

SUPPLEMENTARY INFORMATION

Mean-field and linear regime approach to magnetic hyperthermia of core-shell nanoparticles: Can tiny nanostructures fight cancer?

Marcus S. Carrião and Andris F. Bakuzis*

Instituto de Física, Universidade Federal de Goiás, Goiânia, GO 74001-970 Brazil. E-mail: bakuzis@ufg.br

1 Unit cells per region calculation

If a_c and a_s are the lattice constant of material that compose core and shell, respectively, one can define the thickness of surface and shell interface as a_s , thickness of core interface as a_c , the shell kernel thickness as la_s , where l is arbitrary, and the core kernel diameter can be written in terms of the nanoparticle diameter d as $d_{ck} = d - (4a_s + 2la_s + 2a_c)$. From this, the core kernel volume can be written ($V_{ck} = \pi d_{ck}^3/6$), and so, divided by the volume of the cubic unit cell a_c^3 , it gives the number of unit cells in this subregion. In our approximation we consider the lower integer value. Analogously, the number of unit cells in each subregion can be obtained (see Fig. 2b of main article):

$$N_{ck} = \frac{\pi}{6a_c^3} (d - (4a_s + 2la_s + 2a_c))^3, \quad (S1a)$$

$$N_{ci} = \frac{\pi}{6a_c^3} (d - (4a_s + 2la_s))^3 - N_{ck}, \quad (S1b)$$

$$N_{si} = \frac{\pi}{6a_s^3} (d - (2a_s + 2la_s))^3 - N_{ck} - N_{ci}, \quad (S1c)$$

$$N_{sk} = \frac{\pi}{6a_s^3} (d - (2a_s))^3 - N_{ck} - N_{ci} - N_{si}, \quad (S1d)$$

$$N_{su} = \frac{\pi}{6a_c^3} (d)^3 - N_{ck} - N_{ci} - N_{si} - N_{sk}, \quad (S1e)$$

So one can consider that $N_c = N_{ck} + N_{ci}$, $N_s = N_{si} + N_{sk} + N_{su}$, and $N_T = N_c + N_s$, where N_{ck} , N_{ci} , N_{si} , N_{sk} , and N_{su} are the number of unit cell in core kernel, core interface, shell interface, shell kernel, and surface, respectively. Figure S1 shows the percentage of each region, core and shell, as function of the diameter of nanoparticle.

2 Core-Shell Hamiltonian

The Heisenberg-like Hamiltonian used to describe the nanoparticle sites is

$$\mathcal{H} = -g\mu_B\mu_0 \sum_i \vec{H} \cdot \vec{S}_i - 2 \sum_{i < j} J_{ij} \vec{S}_i \cdot \vec{S}_j, \quad (S2)$$

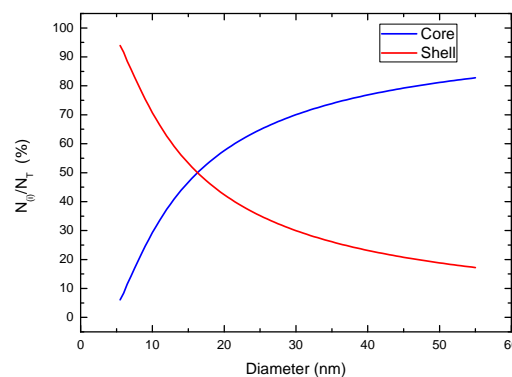


Fig. S1 Percentage of unit cell in each region of nanoparticle as function of diameter.

where i and j run over all sites. If i_c and i_s are counters that run exclusively over core and shell sites, respectively, one can split the Hamiltonian into

$$\mathcal{H} = \left(-g\mu_B\mu_0 \sum_{i_c} \vec{H} \cdot \vec{S}_{i_c} - 2 \sum_{i_c < j} J_{i_c j} \vec{S}_{i_c} \cdot \vec{S}_j \right) \Big|_{\text{core}} + \left(-g\mu_B\mu_0 \sum_{i_s} \vec{H} \cdot \vec{S}_{i_s} - 2 \sum_{i_s < j} J_{i_s j} \vec{S}_{i_s} \cdot \vec{S}_j \right) \Big|_{\text{shell}}. \quad (S3)$$

In first neighbours approximation, j no longer runs over all sites, but only in $i + \delta$, where δ runs over all first neighbours. Thus, a first neighbour j can be at the same region as i or at the other region with the corresponding exchange term. For example, for core sites the first neighbour can be at core kernel (j_{ck}) or core

interface (J_{ci})

$$\mathcal{H}_{\text{core}}^{\text{Exchange}} = - \left(2 \sum_{i_{ck}, \delta} J_{cc} \vec{S}_{i_{ck}} \cdot \vec{S}_{i_{ck} + \delta} \right) \Big|_{\text{core kernel}} + \left(2 \sum_{i_{ci}, \delta} J_{c\delta} \vec{S}_{i_{ci}} \cdot \vec{S}_{i_{ci} + \delta} \right) \Big|_{\text{core interface}}. \quad (\text{S4})$$

If J_{cc} is the exchange constant between sites of core and J_{cs} is the exchange constant between sites of different regions, then $J_{c\delta}$ should assume the corresponding value if the neighbour of core interface site is in core or shell region. This same procedure can be done to shell region. It is important to notice that in Heisenberg Hamiltonian, J is related to the interaction between the spin of atoms. Here, the exchange parameter is related to the exchange interaction between sites, which means unit cells. So, J assumes an *effective* value for the entire unit cell. As well, the spin of the site now corresponds to an effective spin in that region. From this Hamiltonian, the energy of the sites of each region within mean field theory can be written using $\mathcal{H}_l = -S_l E_l$. As an example, specifically to core region:

$$E_c = g\mu_B\mu_0 \sum_{i_c} H + 2 \sum_{i_{ck}, \delta} J_{cc} \langle S_c \rangle + 2 \sum_{i_{ci}, \delta} J_{c\delta} \langle S_\delta \rangle. \quad (\text{S5})$$

The sum in i_c results in N_c , the sum in i_{ck} in N_{ck} , the sum in i_{ci} in N_{ci} , while the sum in δ corresponds to the number of first neighbours. $\langle S_\delta \rangle$ can assume the mean spin value of core $\langle S_c \rangle$ or shell $\langle S_s \rangle$ depending where this neighbour is located. While the mean spin value is calculated from

$$\langle S_l \rangle = \frac{\text{Tr} \left(S_l e^{\frac{S_l E_l}{k_B T}} \right)}{\text{Tr} \left(e^{\frac{S_l E_l}{k_B T}} \right)}, \quad (\text{S6})$$

with Tr the trace over the spin states.

3 Magnetisation description functions

The saturation magnetisation can be defined as a volumetric density of magnetic moments, so for each site (unit cell), one can write:

$$M_S = \frac{g\mu_B S_{\text{eff}}}{a^3}, \quad (\text{S7})$$

where g is the Landé factor, μ_B the Bohr magneton and S_{eff} the effective spin of site. The nanoparticle magnetisation, however, depends on magnetic field and its value depends on magnetisation of core and shell, which are provided by the coupled equations. Thus, one will get each component (M_c and M_s) as function of

mean spin ($\langle S_{(c)} \rangle$ and $\langle S_{(s)} \rangle$), which varies from $-S_{\text{eff}}$ to S_{eff} :

$$\langle S_c \rangle = (N_{ck} \mathcal{F}(E_{ck}) + N_{ci} \mathcal{F}(E_{ci})) / N_c, \quad (\text{S8a})$$

$$\langle S_s \rangle = (N_{su} \mathcal{F}(E_{su}) + N_{sk} \mathcal{F}(E_{sk}) + N_{si} \mathcal{F}(E_{si})) / N_s. \quad (\text{S8b})$$

The equations above are numerically solved. Depending on the number of spin states distinct functions $\mathcal{F}(E)$ are obtained. For spin 1/2, Callen identity is obtained. This function might represent cases with very strong uniaxial anisotropy. When the effective spin is very large, tending to infinity, Langevin is obtained. For any spin value, one finds the Brillouin function ($\mathcal{B}_S(x)$) which varies from -1 to 1 . So, one finds that $\mathcal{F}(x) = S_{\text{eff}} \mathcal{B}_S(x)$, i.e.

$$\mathcal{F}(x) = S_{\text{eff}} \left[\left(1 + \frac{1}{2S_{\text{eff}}} \right) \coth \left(x \left(1 + \frac{1}{2S_{\text{eff}}} \right) \right) + \frac{1}{2S_{\text{eff}}} \coth \left(\frac{x}{2S_{\text{eff}}} \right) \right]. \quad (\text{S9})$$

4 Energy argument of Brillouin Function

From Heisenberg-like Hamiltonian, one can find the energy terms for each subregion sites through mean field theory procedure. The Zeeman contribution is present in all subregions, however, the exchange interaction depends on the environment (number of first neighbours) of the sites. So, these energy arguments of Brillouin function are:

$$E_{ck} = \frac{zJ_{cc}S_{\text{eff}}\langle S_c \rangle + g\mu_B\mu_0 S_{\text{eff}}H}{k_B T}, \quad (\text{S10a})$$

$$E_{ci} = \frac{(z - z')J_{cc}S_{\text{eff}}\langle S_c \rangle + z'J_{cs}S_{\text{eff}}\langle S_s \rangle + g\mu_B\mu_0 S_{\text{eff}}H}{k_B T}, \quad (\text{S10b})$$

$$E_{si} = \frac{(z - z')J_{ss}S_{\text{eff}}\langle S_s \rangle + z'J_{cs}S_{\text{eff}}\langle S_c \rangle + g\mu_B\mu_0 S_{\text{eff}}H}{k_B T}, \quad (\text{S10c})$$

$$E_{sk} = \frac{zJ_{ss}S_{\text{eff}}\langle S_s \rangle + g\mu_B\mu_0 S_{\text{eff}}H}{k_B T}, \quad (\text{S10d})$$

$$E_{su} = \frac{(z - 1)J_{ss}S_{\text{eff}}\langle S_s \rangle + g\mu_B\mu_0 S_{\text{eff}}H}{k_B T}. \quad (\text{S10e})$$

z is the maximum number of first neighbours of a site (in cubic arrangement, 6), while z' is the number of first neighbours of interface sites that are located in the other region (for our case $z' = 1$).

5 Polydisperse Models

In the conventional LRT model, SLP expression have an explicit dependence in diameter d . For this reason, a polydisperse equation

can be found by the integration of

$$SLP_{\text{poly}} = \int_0^{\infty} SLP_{\text{mono}}(d)g(d)dd, \quad (\text{S11})$$

where $g(d)$ is the distribution function of diameter (see Section 9). In the model presented in the main article, for an ensemble core-shell nanoparticles, the diameter is considered to calculate the nanoparticle volume (V_{T}) and the number of unit cells N_i of each region (see eq. 11 of main article). But N_i is necessary to calculate the equilibrium magnetisation of each region ($M_{O(i)}$) and, since the magnetisations are given by two transcendental coupled equations, a direct integration is not possible. Nevertheless, N_i can be written in terms of volume, and therefore can be integrated. That way, the core-shell polydisperse model were obtained from two different integrations: a direct integration of total volume V_{T} (outside of parenthesis in eq. 11) and an integration of N_c and N_s :

$$N_i = \frac{V_i}{a_i^3} = \frac{1}{a_i^3} \int_0^{\infty} V(d)g(d)dd, \quad (\text{S12})$$

which results in a mean value of *polydisperse number of unit cell* for each region. Then, this value is used to calculate M_0 and ϕ for each region (both inside of parenthesis). This type of procedure is similar to a decoupling approximation, where the mean of the product of two functions, κ and η , corresponds to the product of the mean value of each function, i.e. $\langle \kappa \eta \rangle = \langle \kappa \rangle \langle \eta \rangle$.

6 Nanoparticle synthesis

The fluid was synthesised by the co-precipitation of iron and manganese chlorides ($\text{FeCl}_3 \cdot 6\text{H}_2\text{O}$ and $\text{MnCl}_2 \cdot 4\text{H}_2\text{O}$) in methyllamine CH_3NH_2 followed by passivation process with iron nitride $\text{Fe}(\text{NO}_3)_3$ in nitric acid (HNO_3) and a subsequent coating with citrate (from sodium citrate dihydrate, $\text{C}_6\text{H}_5\text{Na}_3\text{O}_7 \cdot 2\text{H}_2\text{O}$).

7 Magnetophoretic experiment

For each sample, a flask containing approximately 4 ml were positioned on a support that lay a few millimetres over a permanent magnet (see Fig. S2). This magnet produces a gradient of magnetic field which interacts with nanoparticles (which are uniformly magnetised single-domains) magnetic moments (\vec{m}), promoting motion due a magnetic force (considering a uniform magnetisation):

$$\vec{F}_m = -\nabla \left(-\vec{m} \cdot \vec{B} \right) = (\vec{m} \cdot \nabla) \vec{B}. \quad (\text{S13})$$

The nanoparticles start to move down, decreasing the distance with the magnet, and increasing the dipolar interaction with it. The magnet, submitted to the reaction force, is pulled up by the fluid in the flask. The weighing scale indicates a decreasing of

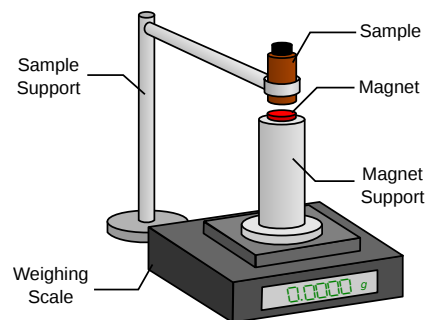


Fig. S2 Scheme of apparent mass magnetophoretic experiment.

the apparent mass of the magnet, which is evidently dependent of magnetic fluid properties. Monitoring this effect over time (see Fig. S3), is possible to identify a saturation process, when hydrodynamic equilibrium is reached. After 92 hours (5520 minutes) of experiment, parts of 200 μl were taken with a micropipette from the top and bottom of the flask.

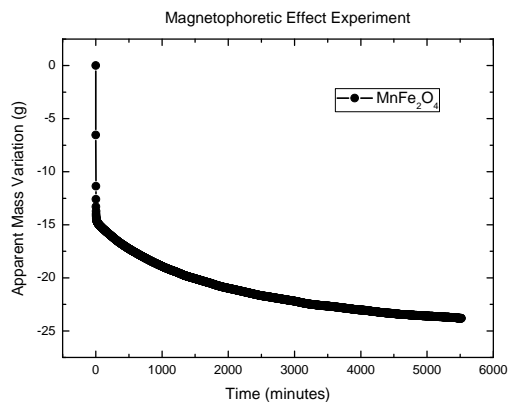


Fig. S3 Magnet apparent mass variation as function of time.

8 Vibrating sample magnetometry

The samples taken from the magnetophoretic experiment have, at least, two distinct properties: concentration and particle size. The first, due the motion of particles towards flask bottom. The second, due different response to gradient of magnetic field. However, for nanostructures, many properties (including magnetisation) are size dependent. Figure S4a shows specific magnetisation curves of powder (obtained after 24 hours drying at 60 °C) of samples, measured in a ADE Magnetics magnetometer, model EV9. If all nanoparticles have the same magnetisation, we should have three identical curves, but it is not the case. Original and Bottom samples present similar behaviours and the difference (around 3%) can be explained by the diameter variation (con-

firmed by TEM, as will be discussed). The Aliquot sample, however, presents a drastically low magnetisation promoted (not only, but also) by diameter decreasing. The process of drying the samples allows to estimate the concentration $x = m_p/v_t$, knowing the total volume dried (v_t) and measuring the mass of remaining powder m_p . We will call this a massic estimation of concentration. The values obtained were 77.1 mg/ml, 15.6 mg/ml and 79.5 mg/ml for Original, Aliquot and Bottom samples, respectively.

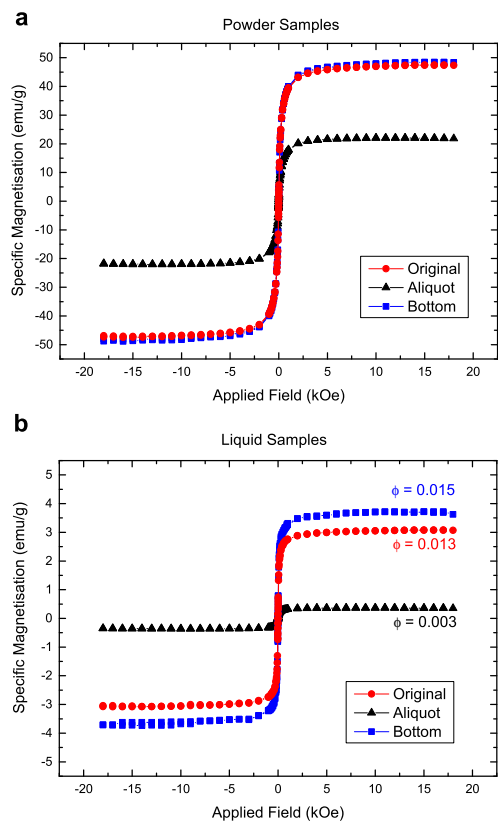


Fig. S4 (a) Specific magnetisation as function of applied field for powder samples. (b) Specific magnetisation as function of applied field for liquid samples, as taken from magnetophoretic experiment.

Liquid samples, as taken from magnetophoretic experiment, were also magnetically characterised. Figure S4b shows the specific magnetisation as function of applied field. Comparing the saturation magnetisation of liquid and powder samples, is possible to determine the volume fraction (ϕ) and then the concentration ($x = \rho\phi$). From this magnetic estimation, the concentrations found were 66.3 mg/ml, 16.5 mg/ml and 76.5 mg/ml for Original, Aliquot and Bottom samples, respectively, which agree with massic estimation. At first glance, from LRT point of view, SLP should not depend on concentration. Nevertheless, some phenomena which affects the heat efficiency (for example, particle-particle interaction) depend on concentration. For this reason we

decide to dilute Original and Bottom samples, to reach Aliquot concentration, before analyse the heating rate curves. The magnetisation curves of samples at same volume fraction can be seen in the main article. Although considered at the same concentration, in reality, the samples present a mean mass concentration of 15.1 ± 1.1 mg/ml, which represent an standard deviation of 7%. This small difference should not affect the heating efficiency. Table S1 shows the experimental magnetisations obtained for the samples.

Sample	M_S (Fig. S4a)	M_S (Fig. S4b)	M_S (Fig. 7a)
	(emu/cm ³) or (kA/m)		
Original	242.1 ± 0.5	15.6 ± 0.5	3.4 ± 0.5
Aliquot	111.1 ± 0.5	1.8 ± 0.5	1.8 ± 0.5
Bottom	248.2 ± 0.5	19.0 ± 0.5	3.8 ± 0.5

Table S1 Experimental M_S values for powder, fluid samples at different concentrations (as acquired from magnetophoretic experiment) and fluid samples at same concentration (15.1 ± 1.1 mg/ml).

9 Transmission electron microscopy

The TEM images were obtained in LabMic (www.labmic.ufg.br) facilities using a JEOL JEM-2100 microscope. Samples were diluted in isopropyl alcohol and dropped on copper grids (coated with carbon films) and dried. Figures S5a, S5b and S5c shows an example of image used to measure nanoparticles size and Fig. S6d shows another image, in higher magnification, of MnFe₂O₄ nanoparticles. With help of open source program ImageJ, maintained by National Institute of Health (www.imagej.nih.gov), diameter of the nanoparticles were measured and disposed in histograms, fitted by log-normal distribution:

$$g(d) = \frac{1}{d\delta\sqrt{2\pi}} \exp\left[-\frac{\ln(d/d_m)^2}{2\delta^2}\right]. \quad (\text{S14})$$

Sample	Counts	d_m (nm)	δ
Original	523	11.1 ± 0.1	0.29 ± 0.01
Aliquot	490	8.2 ± 0.2	0.27 ± 0.03
Bottom	535	12.7 ± 0.4	0.38 ± 0.03

Table S2 Parameters of log-normal fitting.

Table S2 shows the log-normal fitting parameters for each sample. From the fitting, the mean diameter $\bar{d} = d_m \exp(\delta^2/2)$ and standard deviation $SD = ((\exp(\delta^2) - 1) d_m^2 \exp(\delta^2))^{1/2}$ were calculated. The size histograms, number of counts and log-normal fitting parameters can be seen in the main article.

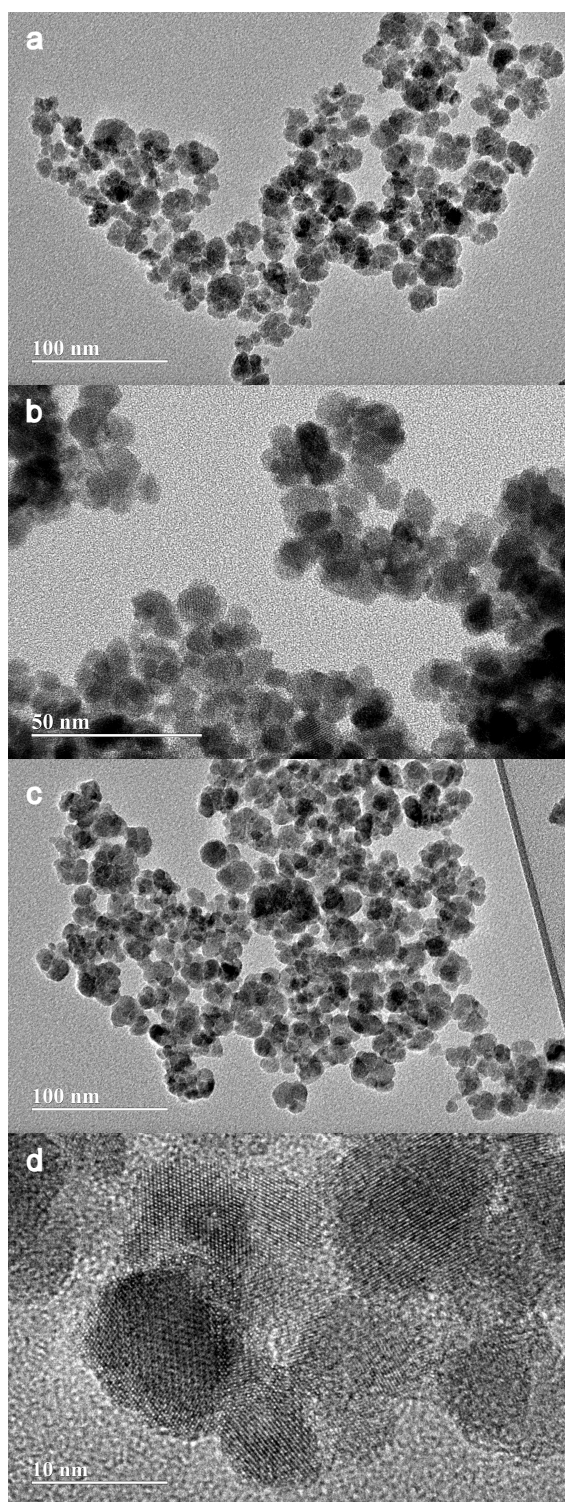


Fig. S5 Low magnification TEM images of nanoparticles in samples (a) Original, (b) Aliquot, (c) Bottom, and (d) high magnification image of sample Original.

10 Magnetic hyperthermia experiment

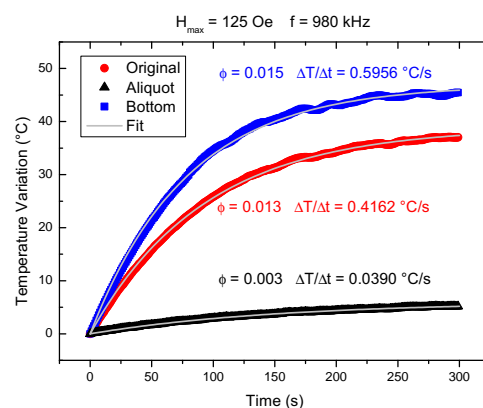


Fig. S6 Temperature variation as function of time in magnetic hyperthermia of liquid samples (as taken from magnetophoretic experiment).

Using approximately 100 μl , liquid samples were submitted to magnetic hyperthermia procedure in a nanoTherics equipment, model magneTherm, applying alternating magnetic fields of amplitude 125 Oe (9.9 kA/m) and frequency 980 kHz. The temperature was monitored with optical fibre thermometer. Figure S6 shows the temperature variation as function of time in magnetic hyperthermia of liquid samples with the concentration acquired from magnetophoretic experiment. When compared with temperature variation at same concentration (that can be seen in main article), becomes evident the influence of concentration in heating rate. These curves were fitted using a Box-Lucas function ($T(t) = a(1 - e^{-bt})$) from which is possible to obtain the heating rate $(dT/dt)_{t \rightarrow 0} = ab$.

11 LRT versus Core-Shell model

Although both LRT and our core-shell model are used to describe properties of the same type of system, i.e. magnetic nanoparticles, there is a difficulty associated to do a fair comparison between them. It comes from the fact that they were designed from different concepts of systems. LRT is *homogeneous* in all meanings: the nanoparticle properties (M_S , K , α , ρ , etc) are macroscopic mean values and do not depend on nanoparticle internal structure, diameter, etc. This means that, for some theoretical calculations, properties are overestimated or underestimated. To exemplify that, consider the calculation of theoretical *SLP* as function of diameter for some sample. In LRT approach, the magnetisation (as many other parameters) is assumed as independent of diameter, when it actually is not. Thus, magnetisation will be overestimated for small nanoparticles and underestimated to larger ones. One way skip this problem is assume our core-shell de-

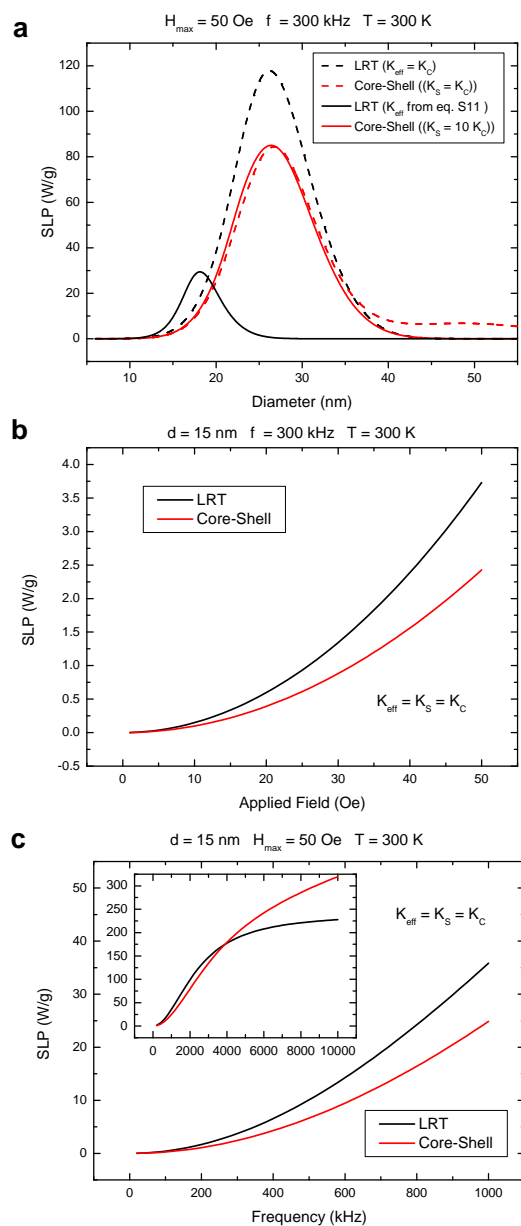


Fig. S7 (a) *SLP* as function of diameter for LRT and core-shell model, considering the diameter dependent of magnetisation, when $K_{\text{eff}} = K_s = K_c$ (dashed lines) and K_{eff} follows Eq. (S15). (b) *SLP* as function of applied field for LRT and core-shell model. (c) *SLP* as function of frequency for LRT and core-shell model. In the inset, same dependence for higher frequency values, approaching saturation. The parameters used here correspond to *soft* material, as shown in Table 1 of main article.

scription of magnetisation ($M_S(d)$) as a input to LRT. Figure S7a shows (as dashed lines) LRT and our core-shell model results in this case. As discussed along the article, the considerations of our core-shell model increase the *SLP* of small nanoparticles, and

decrease the *SLP* around optimum diameter (which provide maximum *SLP*). Now, consider that this study of *SLP* as function of diameter will take into account the surface anisotropy (which could be needed to explain measured K above bulk values). Once more, a nanoparticle property (in this case, anisotropy) is assumed as independent of diameter. However, the surface anisotropy contribution should increase while diameter decreases (since surface-volume ratio increases). One could perform this simulation, but (once more) anisotropy will be overestimated or underestimated, depending on size. We could try to do the same procedure described above for magnetisation, using K_c and K_s (which are proportional to D_c and D_s) of our core shell model to estimate the equivalent effective anisotropy K_{eff} of LRT. A way to do that is consider $K_{\text{eff}} = K_{\text{vol}} + (6/D)K_{\text{sur}}$, where K_{vol} represents the volumetric anisotropy contribution and K_{sur} the surface anisotropy contribution. Usually, K_{vol} assumes the *bulk* value, but here it will be considered equal to core-shell model's K_c , for comparison. On the other hand, K_{sur} and K_s have different units, and to correct this, one could compare the anisotropy energies involved $V_s K_s = K_{\text{sur}} S_{\text{np}}$, where S_{np} is the nanoparticle surface area. Finally, the K_{eff} of LRT in terms of core-shell model properties can be written:

$$K_{\text{eff}} = K_c + \frac{N_s}{N_T} K_s. \quad (\text{S15})$$

Figure S7a shows (in solid lines) a comparison of LRT and core-shell model considering $K_s = 10K_c$. One can see that, as discussed in main article, anisotropy changes in core-shell model implies in shifts of each contribution peak. While, in LRT some kind of change will imply in major modifications (similar to the changes promoted by dipolar interaction, see Ref. 18 of main article). Again, it is clear that the foundation of these two models are quite different: one is based on uniformity of nanoparticles and the other on interaction between nanoparticles elements (regions, unit cells, etc). The existence of two peaks in core-shell model is naturally expected, since one have two regions (which somehow act like two separated but interdependent systems). On the other hand, in LRT not even all these modifications described above are sufficient to provide similar results. After all, within a range of acceptable parameters, LRT and core-shell model have some similarities, like optimum diameter (see dashed lines in Fig. S7a); the dependence with applied field (see Fig. S7b); and the dependence with the frequency (see Fig. S7c). However, the most important similarity is the validity limit. Both models are based on linear response, but described in terms of different parameters. The definition of the validity range is often related to $\xi < 1$ and all critics applied to LRT (except homogeneity, obviously) could also be made to core-shell model (see Ref. 38 of main article).

12 Model calculation

All calculations were performed using Maple 13 software.

13 Shell thickness study

In main article, magnetisation and *SLP* were studied as function of diameter (see Fig. 5c and 5d). The curves were shown in diameter scale and the upper axis showed the equivalent N_s/N_T fraction. Since the relation between diameter and N_s/N_T is not linear, is convenient to present a alternative version of these curves, as showed in Fig. S8.

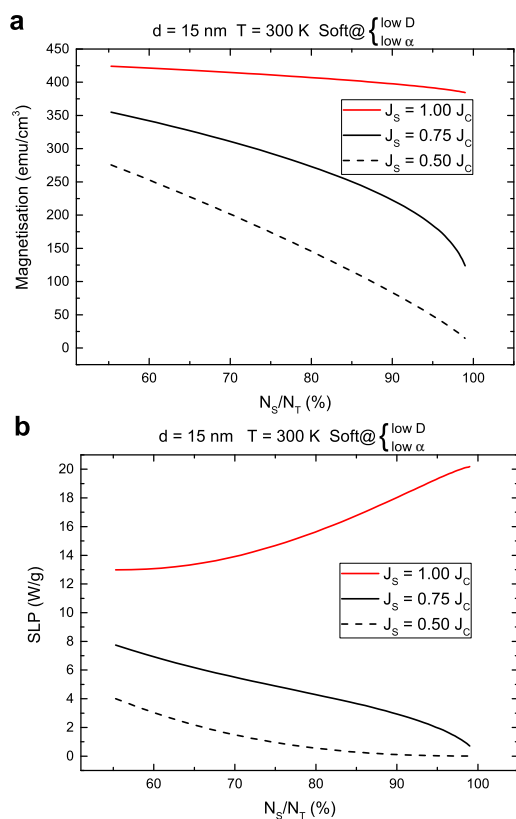


Fig. S8 (a) Magnetisation as function of N_s/N_T for different J_c/J_s ratio. (b) *SLP* as function of N_s/N_T for different J_c/J_s ratio. Alternative scale of Fig. 5c and 5d of main article.